INTERNATIONAL JOURNAL FOR NUMERICAL METHODS IN FLUIDS, VOL. 7, 953–984 (1987)

LAGRANGIAN FINITE ELEMENT ANALYSIS APPLIED TO VISCOUS FREE SURFACE FLUID FLOW

BALASUBRAMANIAM RAMASWAMY* AND MUTSUTO KAWAHARA†

Department of Civil Engineering, Chuo University, 13–27, Kasuga 1-Chome, Bunkyo-ku, Tokyo 112, Japan

SUMMARY

A new Lagrangian finite element formulation is presented for time-dependent incompressible free surface fluid flow problems described by the Navier–Stokes equations. The partial differential equations describing the continuum motion of the fluid are discretized using a Galerkin procedure in conjunction with the finite element approximation. Triangular finite elements are used to represent the dependent variables of the problem. An effective time integration procedure is introduced and provides a viable computational method for solving problems with equality of representation of the pressure and velocity fields. Its success has been attributed to the strict enforcement of the continuity constraint at every stage of the iterative process. The capabilities of the analysis procedure and the computer programs are demonstrated through the solution of several problems in viscous free surface fluid flow. Comparisons of results are presented with previous theoretical, numerical and experimental results.

KEY WORDS Navier–Stokes equations Lagrangian method Finite element method Galerkin formulation Linear interpolation Free surface

INTRODUCTION

This paper presents the development of a new scheme to simulate numerically the two-dimensional flow of an incompressible fluid with a free surface. In recent years, many methods have been developed for calculating the steady as well as the transient dynamics of incompressible fluids with free surfaces. The most widely used of these has been the marker and cell (MAC) technique developed by Harlow and Welch[1] and further refined by many others.[2–6] While a number of variations of this technique have been used to solve a wide variety of problems, methods using the MAC technique have the disadvantage of requiring a considerable amount of core storage. Recently, a great number of research papers[7–17] have been published on the free surface of viscous flow problems and finite element techniques have been applied successfully to their numerical analyses. In these papers, most of the work is carried out by assuming the flow to be steady or the change in time to be not intensive. In addition, there has been an extended effort to use a hybrid method to solve this type of problem.[18–20] A partial list of developers for the analysis of free surface flow by finite difference as well as finite element methods based on the two-dimensional potential function is given in References 21 and 22. Even though the Eulerian potential problem needs only one variable, the potential ϕ in either two or three space dimensions, its main disadvantage is the requirement of numerical differentiation to obtain the velocities.

---

* Graduate student.
† Professor.

0271–2091/87/090953–32$16.00

Received 15 December 1986

Until very recently, finite element solutions of unsteady, free surface flow invariably employed the Eulerian description of the motions. In this description, the mesh of elements remains fixed relative to the observer, while the fluid moves through the mesh with time. In a strict application of the method, each element is forced to be homogeneous in that it is characterized by uniform density, pressure, velocity and type of material. This method has the tremendous advantage of being able to handle extreme fluid distortions, but the material interfaces may become hard to identify. The method also suffers from the inability to resolve fine structures which move with the fluid, unless the entire mesh of elements is made so fine that numerical calculations become impracticable.

To circumvent the above-mentioned difficulties associated with free boundaries in Eulerian methods, this paper deals in detail with the finite element technique combined with the Lagrangian description. In the following, it will be demonstrated how a Lagrangian finite element method may be implemented for an incompressible Newtonian liquid. In the present approach, the domain is assumed to be covered by a mesh of triangular finite elements whose vertices move with the fluid. In this process, fluid in the interior of a finite element always remains in that element and fluid boundaries always move with the element boundaries. In an incompressible Lagrangian calculation, the volume of each element must remain constant during the course of a calculation. To satisfy this constraint, an effective splitting-up time discretization procedure is employed. In this splitting-up method, an auxiliary velocity field is computed first, which accounts for all contributions to the acceleration, except pressure, and satisfies the velocity boundary conditions. Then, the final velocities are evaluated by adding to the auxiliary velocities pressure contributions which are computed to satisfy the incompressibility condition. This method provides the most promise for obtaining Lagrangian finite element solutions to the Navier–Stokes equations with equal-order pressure and velocity field representations. Although the Lagrangian method is not applicable to flows undergoing large distortions, where meshes can be twisted into unacceptable shapes, its advantage is the ease with which it handles free surfaces and interfaces, which makes it applicable to a wide variety of problems. In the authors' opinion, the resulting method is quite competitive with existing finite difference methods and at the same time offers significant advantages over both existing Lagrangian finite difference and finite element methods.

Examples of problems investigated by the present computing technique are (1) the breaking of a dam, (2) the Rayleigh–Taylor instability of a falling free surface and (3) the non-linear oscillation. All these problems are two-dimensional in nature. The present results are compared with those which are available in the literature and are based on alternative approaches for treating incompressibility constraint and convective acceleration terms. From comparative studies, it is concluded that the present approach based on the Lagrangian formulation has great advantages for the analysis of fluid flow with surfaces.

BASIC EQUATIONS

Throughout this paper, the equations are described using indicial notation and the summation convention for repeated indices. The problem under consideration is the unsteady motion of a surface wave under gravity in a rectangular tank. Let V be the fluid domain which is surrounded by a piecewise smooth boundary S. To illustrate the fluid mechanical content of the formulation, the equations of conservation of momentum and mass for incompressible Newtonian fluids in the conventional Eulerian form are given by the Navier–Stokes equation and the equation of continuity as follows:

$$\rho \left.\frac{\partial v_i}{\partial t}\right|_{x_i} + \rho v_j v_{i,j} = \sigma_{ij,j} + \rho f_i \quad \text{in } V, \tag{1}$$

$$v_{i,i} = 0 \quad \text{in } V. \tag{2}$$

Here $v_i = v_i(\mathbf{x}, t)$ are the components of the velocity field in a spatial co-ordinate system $x_i (i = 1, 2)$, $\mathbf{x}$ is used as shorthand for (x_1, x_2), ρ is the fluid density, $f_i (t = 1, 2)$ are the components of the gravitational acceleration and t is the time. The total stress tensor σ_{ij} is given by

$$\sigma_{ij} = -p\delta_{ij} + \mu(v_{i,j} + v_{j,i}), \tag{3}$$

where p is the pressure and μ is the coefficient of viscosity. The position vector for a fluid element, $\mathbf{x}$, satisfies the equation

$$\mathrm{d}\mathbf{x}/\mathrm{d}t = \mathbf{v}. \tag{4}$$

The left-hand side of equation (1) is the total convective derivative of v_i, which represents the time rate of change of v_i in a fluid element moving with the fluid; i.e., it is the time rate of change for a Lagrangian fluid element. Therefore the governing equations for the Lagrangian formulation are given by

$$\rho \left.\frac{\partial v_i}{\partial t}\right|_{X_i} = \sigma_{ij,j} + \rho f_i \quad \text{in } V, \tag{5}$$

$$v_{i,i} = 0 \quad \text{in } V, \tag{6}$$

where $|_{X_i}$ indicates the material co-ordinates X_i are held constant in taking the time derivative. In this formulation, the co-ordinates x_i appear as dependent variables and the independent variables are instead fluid particle labels. The particle labels are conveniently defined by the initial location of the fluid particles x_i^0 at reference time t_0. The co-ordinates, when viewed as functions of particles and time, are then expressed as the displacement functions $x_i = x_i(x_i^0, t_0, t)$, where $x^0 = (x_1^0, x_2^0)$. If the fluid particle is defined as $P_K = P_K(x_i^0, t_0)$, then the velocity vectors, pressure field and position of each fluid particle P_K with the initial location x_i^0 at time t_0 are defined by

$$\left.\begin{aligned} v_i^n &= v_i(P_K, t^n) && (7a)\\ p^n &= p(P_K, t^n) && (7b)\\ x_i^n &= x_i(P_K, t^n) && (7c) \end{aligned}\right\} \text{ at time } t^n$$

and

$$\left.\begin{aligned} v_i^{n+1} &= v_i(P_K, t^{n+1}) && (8a)\\ p^{n+1} &= p(P_K, t^{n+1}) && (8b)\\ x_i^{n+1} &= x_i(P_K, t^{n+1}) && (8c) \end{aligned}\right\} \text{ at time } t^{n+1}.$$

The Lagrangian velocity field is related to the co-ordinates by the definition

$$\partial x_i(P_K, t)/\partial t = v_i(P_K, t). \tag{9}$$

The dependent variables in the present analysis are the Lagrangian velocity field v_i and the Lagrangian pressure field p.

To complete the formulation of the basic equations, a set of boundary and initial conditions is required. The continuum boundary conditions are of two types those specifying velocity and those specifying stress. Application of the specified velocity condition in discrete form is straightforward. The equation for the particular velocity component at a boundary node is replaced by a constraint condition enforcing the proper boundary value. The rigid wall boundary conditions are the simplest to derive they follow directly from the momentum equations. For a free-slip wall, the normal velocity must vanish; for a no-slip wall, the tangential components must, in addition,

vanish. These conditions in general can be defined as

$$v_i = \hat{v}_i \quad \text{on} \quad S_2, \tag{10}$$

where the superposed ^ denotes the function which is given on the boundary.

Boundary conditions at the free surface S_1 remains the most interesting of these two conditions. For the numerical method, they are the most difficult conditions to apply accurately. The principles that form the basis for the free surface boundary conditions are stated as follows:

(1) Stress tangential to the surface must vanish.
(2) Stress normal to the surface must exactly balance any externally applied normal stress.

These conditions are expressed as

$$t_i = \sigma_{ij} n_j = \hat{t}_i \quad \text{on} \quad S_1 \tag{11}$$

where n_j is the direction cosine of the outward normal on the boundary with respect to the x_j axis. In the present analysis, $\hat{t}_i$ is assumed to be zero. Moreover, S_1 and S_2 are two disjoint non-overlapping subsets of the boundary S.

In the case of Lagrangian free fluid boundary, the time evolution of the height function is governed by a kinematic equation expressing the fact that the free surface must move with the fluid

$$\partial \eta / \partial t|_{X_i} = 0, \tag{12}$$

where η is the surface elevation measured from the fundamental fluid level. It is clear that equation (12) is Lagrangian in both vertical and horizontal directions.

The initial conditions for the present Lagrangian Navier–Stokes problem consist of specifying the values of velocity and pressure at the initial time.

$$v_i(x_i, 0) = v_i^0(x_i), \tag{13}$$

$$p(x_i, 0) = p^{(0)}(x_i), \tag{14}$$

with the initial velocity $v_i^{(0)}(x_i)$ satisfying the incompressibility condition

$$v_{i,i}^{(0)} = 0. \tag{15}$$

BASIC CONCEPTS OF THE LAGRANGIAN METHOD

In order to implement a numerical solution procedure for the Lagrangian formulation, it is necessary to discretize time and fluid material. The basic concept of the analysis presented in this section is the idea that the material time derivative can be determined approximately by the functions known at both deformed and undeformed positions during a short time increment. The function at the deformed position cannot be obtained before computation; thus an iterative computation is necessary. Assume the total time interval is divided into many short time increments, denoted by Δt, and the fluid is discretized into many triangular finite elements.

The material acceleration is the time derivative for the change of location of a fluid particle. It can be approximated by the increment of velocity using equations (7) and (8) as in the following form:

$$\partial v_i / \partial t|_{X_i} \simeq (v_i^{n+1} - v_i^n)/\Delta t. \tag{16}$$

The location of a nodal point after the increment Δt is given

$$x_i(P_K, t^{n+1}) = x_i^n + \int_{t'=t_n}^{t^{n+1}} v_i(P_K, t')\mathrm{d}t'. \tag{17}$$

The discretization of time is performed by using the following approximation for the integral in equation (17):

$$\int_{t'=t^n}^{t^{n+1}} v_i(P_K, t')\mathrm{d}t' \simeq \tfrac{1}{2}(v_i^{n+1} + v_i^n)(t^{n+1} - t^n). \tag{18}$$

Introducing equation (18) into equation (17), the equation for updating the co-ordinates can be obtained

$$x_i(P_K, t^{n+1}) \equiv x_i^{n+1} \simeq x_i^n + \tfrac{1}{2}\Delta t(v_i^{n+1} + v_i^n). \tag{19}$$

Since the location of a particle, x_i^{n+1}, is a function of v_i^{n+1}, which is not known *a priori*, the finite element analysis based on equation (19) must be solved by some iterative procedure which must be repeated in every time step. The algorithm for an iterative process is briefly explained in the following lines.

Let v_i^n, p^n, f_i^n and x_i^n, the velocity, pressure, body forces and nodal co-ordinate values, be known at time t^n. From v_i^n, f_i^n, p^n, x_i^n and boundary specifications, the fields v_i^{n+1}, p^{n+1} and x_i^{n+1} are calculated as follows. At the initial step of iteration, velocity $v_i^{n+1(0)}$, pressure $p^{n+1(0)}$ and position $x_i^{n+1(0)}$ are computed as

$$\tilde{v}_i^{n+1(0)} = \tilde{g}_i(v_i^n, f_i^n, x_i^n), \tag{20}$$

$$p^{n+1(0)} = h(\tilde{v}_i^{n+1(0)}, x_i^n), \tag{21}$$

$$v_i^{n+1(0)} = g_i(\tilde{v}_i^{n+1(0)}, p^{n+1(0)}, x_i^n) \tag{22}$$

$$x_i^{n+1(0)} \simeq x_i^n + \Delta t\, v_i^n, \tag{23}$$

where $\tilde{v}_i^{n+1(0)}$ and $v_i^{n+1(0)}$, for example, mean the value of the intermediate and final velocity components at the initial step of iteration in the $(n+1)$th time interval; g_i and h mean that the velocity and pressure can be computed following the time discretization procedure (explained later) based on the previously known velocity v_i^n and body forces f_i^n at position x_i^n and at time t^n. At the mth iteration cycle (where $m = 1, 2, \ldots$; is the maximum number of iterations), the values are updated by the following equations:

$$\tilde{v}_i^{n+1(m)} = \tilde{g}_i(v_i^n, f_i^n, x_i^{n+1(m-1)}), \tag{24}$$

$$p^{n+1(m)} = h(\tilde{v}_i^{n+1(m)}, x_i^{n+1(m-1)}), \tag{25}$$

$$v_i^{n+1(m)} = g_i(\tilde{v}_i^{n+1(m)}, p^{n+1(m)}, x_i^{n+1(m-1)}), \tag{26}$$

$$x_i^{n+1(m)} \simeq x_i^n + \tfrac{1}{2}\Delta t(v_i^{n+1(m)} + v_i^n). \tag{27}$$

Equations (25) and (26) specify that the velocity and pressure can be computed using the latest positions of the fluid particles. The iteration is repeated until the computed velocity satisfies the following convergence criterion:

$$|v_i^{n+1(m)} - v_i^{n+1(m-1)}| < \varepsilon, \tag{28}$$

where ε is a previously defined small value. If the process converges, then the Lagrangian variables are given by

$$v_i^{n+1} = v_i^{n+1(m)}, \tag{29}$$

$$p^{n+1} = p^{n+1(m)}, \tag{30}$$

$$x_i^{n+1} = x_i^{n+1(m)}. \tag{31}$$

In practical applications, the maximum number of iteration cycles in each time step was 2–3 for normal computation. Thus the velocity and pressure for the change of position of a fluid particle can be computed. The computation is repeated for all $n = 1, 2, \ldots$, where N is the total number of time points.

WEIGHTED RESIDUAL FORMULATIONS

A weak formulation of problem (5)–(15) is obtained by multiplying the differential equations by suitable weighting functions and integrating over a domain V which is bounded by a surface S with a unit normal n_i. Multiply the momentum equation (5) by the weighting function v_i^* and the continuity equation (6) by the weighting function q^* and then integrate over V. After integration by parts of the stress term, use of the divergence theorem and of the boundary condition (11), the following weak form of the original problem is obtained

$$\int_V \left(v_i^* \frac{\partial v_i}{\partial t} \right) \mathrm{d}V = \int_V (v_{i,i}^* p)\,\mathrm{d}V - \nu \int_V [v_{i,j}^* (v_{i,j} + v_{j,i})]\,\mathrm{d}V + \int_V (v_i^* f_i)\,\mathrm{d}V + \int_S \{v_i^* [-p\delta_{ij} + \nu(v_{i,j} + v_{j,i})] n_j\}\,\mathrm{d}S, \tag{32}$$

$$\int_V (q^* v_{i,i})\,\mathrm{d}V = 0, \tag{33}$$

with

$$v_i = \hat{v}_i \quad \text{on} \quad S_1, \tag{34}$$

$$v_i(x_i, 0) = v_i^{(0)}(x_i). \tag{35}$$

Under suitable smoothness conditions for the boundary data $\hat{v}_i$ and $\hat{t}_i$, the Navier–Stokes problem (32)–(35) admits at least one solution.

TIME DISCRETIZATION

In order to implement a numerical solution procedure for the Lagrangian formulation in this paper, the momentum equation and the incompressibility constraint of the Navier–Stokes problem are treated in two phases. This section describes how to compute $\tilde{g}_i$, h and g_i in equations (20)–(22), which in turn help to compute $\tilde{v}_i$, p and v_i in equations (24)–(26).

Phase I: Explicit Lagrangian calculation

Denoting the exact velocity and pressure during the $(n+1)$th time instant by v_i^{n+1} and p^{n+1}, then the following equation are valid:

$$v_i^{n+1} = v_i^n - \Delta t [p_{,i}^{n+1} - \nu(v_{i,j}^n + v_{j,i}^n)_{,j} - f_i^n], \tag{36}$$

$$v_{i,i}^{n+1} = 0. \tag{37}$$

At first, an intermediate Lagrangian nodal velocity field $\tilde{v}_i^{n+1}$, not satisfying the incompressibility constraint, is derived from the previous cycle's velocity vectors, position vectors and body forces by employing a purely explicit Eulerian first-order scheme

$$\int_{V^{n+1}} (v_i^* \tilde{v}_i^{n+1})\,\mathrm{d}V = \int_{V^n} (v_i^* v_i^n)\,\mathrm{d}V - \Delta t\Bigg[\int_{V^n} (v_i^* f_i^n)\mathrm{d}V + \nu\Bigg(\int_{V^n} (v_{i,j}^* v_{i,j}^n)\mathrm{d}V + \int_{V^n} (v_{i,j}^* v_{j,i}^n)\mathrm{d}V\Bigg) - \nu\Bigg(\int_{S^n} (v_i^* v_{i,j}^n + v_i^* v_{j,i}^n) n_j \mathrm{d}S\Bigg)\Bigg], \tag{38}$$

$$\tilde{v}_i^{n+1} = \hat{v}_i \quad \text{on} \quad S_2. \tag{39}$$

The velocity field $\tilde{v}_i^{n+1}$ obtained from equation (38) does not satisfy the incompressibility condition, because it is derived from a discretized version of the weak form of the momentum equation in which the pressure terms are omitted.

Phase II: Implicit Lagrangian calculation

The main objective of the present implicit Lagrangian phase is to obtain the exact velocity which satisfies the incompressibility constraint that has been accelerated by pressure forces at the advanced time level. Once the intermediate velocity has been computed from equation (38), the end-of-step velocity v_i^{n+1} is obtained by adding to $\tilde{v}_i^{n+1}$ the dynamical effect of the still unknown pressure p^{n+1}, which is to be determined so that the weak form (33) of the incompressibility condition remains satisfied

$$\int_{V^{n+1}} (v_i^* v_i^{n+1})\,\mathrm{d}V = \int_{V^{n+1}} (v_i^* \tilde{v}_i^{n+1})\,\mathrm{d}V - \Delta t \int_{V^{n+1}} (v_i^* p_{,i}^{n+1})\,\mathrm{d}V, \tag{40}$$

$$\int_{V^{n+1}} (q^* v_{i,i}^{n+1})\,\mathrm{d}V = 0. \tag{41}$$

Taking divergence on both sides of equation (40), together with the incompressibility constraint $v_{i,i}^{n+1} = 0$, the following linear system of equations which governs the pressure field can be derived

$$\int_{V^{n+1}} (q^* p_{,ii}^{n+1})\,\mathrm{d}V = (1/\Delta t) \int_{V^{n+1}} (q^* \tilde{v}_{i,i}^{n+1})\,\mathrm{d}V. \tag{42}$$

The left-hand side of equation (42) contains derivatives of second order which may be reduced to first order through an integration by parts. Equation (42) is then

$$\int_{V^{n+1}} (q_{,i}^* p_{,i}^{n+1})\,\mathrm{d}V = -(1/\Delta t) \int_{V^{n+1}} (q^* \tilde{v}_{i,i}^{n+1})\,\mathrm{d}V + \int_{S^{n+1}} (q^* p_{,i}^{n+1} n_i)\,\mathrm{d}S, \tag{43}$$

where the divergence theorem has been used to obtain the boundary integral. Based on the authors' experience with numerous applications of this method to a diverse range of problems, the above equation possesses no particular difficulty in solution and does not produce any spurious pressure or chequer-boarding. To solve equation (43), the following boundary conditions are applied:

$$p^{n+1} = 0 \quad \text{on} \quad S_1, \tag{44}$$

$$p_{,i}^{n+1} n_i = 0 \quad \text{on} \quad S_2. \tag{45}$$

Once the pressure has been determined from equation (43), Lagrangian velocities are calculated from equation (40). Finally, the vertex co-ordinates are moved according to equation (19). This completes the updating of all quantities.

FINITE ELEMENT METHOD

The fully discrete form of problems (36)–(45) is obtained by discretizing the domain V into non-overlapping subregions called finite elements. In each element, the unknown fields are approximated by simple polynomial functions. For the present class of problems, let the velocity and pressure be represented within an element by

$$v_i = \Phi_\alpha v_{\alpha i}, \tag{46}$$

$$p = \Phi_\alpha p_\alpha; \tag{47}$$

then the corresponding weighting functions are

$$v_i^* = \Phi_\alpha v_{\alpha i}^*, \tag{48}$$

$$p^* = \Phi_\alpha p_\alpha^*, \tag{49}$$

where Φ_α is the interpolation function, $v_{\alpha i}$ represents the nodal value of the velocity at the αth node of the finite element in the ith direction and $v_{\alpha i}^*$ is the nodal value of the corresponding weighting function p_α is the nodal value for pressure at the αth node of the finite element and p_α^* is the nodal value of the corresponding weighting function. Substituting equation (46)–(49) into (40), (42) and (43) and considering the arbitrariness of the weighting functions, the finite element equations can be derived as follows:

$$\bar{M}_{\alpha\beta}^{n+1}\tilde{v}_{\beta i}^{n+1} = \bar{M}_{\alpha\beta}^{n} v_{\beta i}^{n} - \Delta t(S_{\alpha i\beta j}^{n} v_{\beta j}^{n} - N_\alpha^n f_{\alpha i}^n - \hat{\Omega}_{\alpha i}^n), \tag{50}$$

$$A_{\alpha\beta}^{n+1} p_\beta^{n+1} = -(1/\Delta t) H_{\alpha i\beta}^{n+1}\tilde{v}_{\beta i}^{n+1} + \hat{\Sigma}_\alpha^{n+1}, \tag{51}$$

$$\bar{M}_{\alpha\beta}^{n+1} v_{\beta i}^{n+1} = \bar{M}_{\alpha\beta}^{n+1}\tilde{v}_{\beta i}^{n+1} - \Delta t H_{\alpha i\beta}^{n+1} p_\beta^{n+1}, \tag{52}$$

where

$$M_{\alpha\beta}^n = \int_{V^n} (\Phi_\alpha^n \Phi_\beta^n)\,\mathrm{d}V,$$

$$M_{\alpha\beta}^{n+1} = \int_{V^{n+1}} (\Phi_\alpha^{n+1}\Phi_\beta^{n+1})\,\mathrm{d}V,$$

$$H_{\alpha i\beta}^{n+1} = \int_{V^{n+1}} (\Phi_{\alpha,i}^{n+1}\Phi_\beta^{n+1})\,\mathrm{d}V,$$

$$A_{\alpha\beta}^{n+1} = \int_{V^{n+1}} (\Phi_{\alpha,i}^{n+1}\Phi_{\beta,i}^{n+1})\,\mathrm{d}V,$$

$$N_\alpha^n = \int_{V^n} (\Phi_\alpha^n)\,\mathrm{d}V,$$

$$\hat{\Omega}_{\alpha i}^{n+1} = \int_{S^{n+1}} [\Phi^{n+1} v(v_{i,j}^{n+1} + v_{j,i}^{n+1}) n_j]\,\mathrm{d}S,$$

$$\hat{\Sigma}_\alpha^{n+1} \int_{S^{n+1}} (\Phi_\alpha^{n+1} p_{,i}^{n+1} n_j)\,\mathrm{d}S,$$

$$S_{\alpha i\beta j}^n = v\left(\int_{V^n} (\Phi_{\alpha,k}\Phi_{\beta,k}^n)\delta_{ij}\,\mathrm{d}V + \int_{V^n} (\Phi_{\alpha,i}^n \Phi_{\beta,j}^n)\,\mathrm{d}V\right).$$

In equations (50) and (52), $\bar{M}_{\alpha\beta}$ means the lumped mass matrix obtained simply by summing across each row of the consistent mass matrix $M_{\alpha\beta}$ and placing the results in the diagonal.

The overall iterative solution method is illustrated in Figure 1. Unlike most previous finite

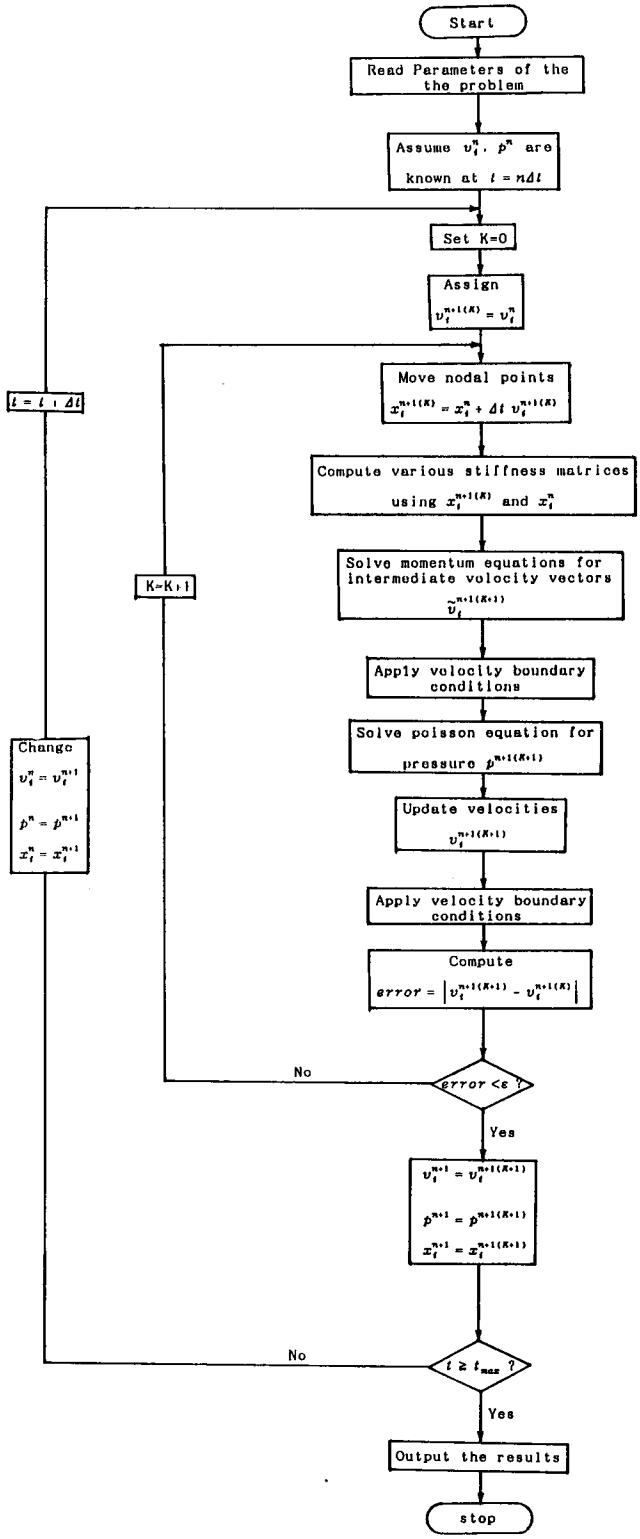

Figure 1. Overall solution method

element methods, the current formulation uses a segregated solution approach; i.e., the velocities and pressure are solved for in a sequential manner rather than simultaneously. The use of a segregated solution results in a considerable saving of storage and execution time and allows for practical size problems to be treated. As indicated in Figure 1, this overall cycle is repeated for as much elapsed time as desired.

NUMERICAL EXAMPLES

Broken dam problem

In this example, a rectangular column of water in hydrostatic equilibrium is confined between two vertical walls, as shown in Figure 2. The water column is 3·5 units wide and 7·0 units high. Gravity is acting downwards with unit magnitude. The dam holding the reservoir is removed instantaneously at time $t = 0$ and the liquid falls away under the force of gravity. The total numbers of nodal points and finite elements are 225 and 392 respectively. Figures 3–7 show a typical sequence of mesh configuration, velocity and pressure plots for the broken dam. From these figures it can be seen that the front of the wave is much retarded in its initial motion and lacks the long sharp tip predicted by analysis. Experimental results for this problem have been reported for the position versus time of the leading edge of the water as it flows to the right (Figure 8). This is a good test problem because it has simple boundary conditions and simple initial configuration. The

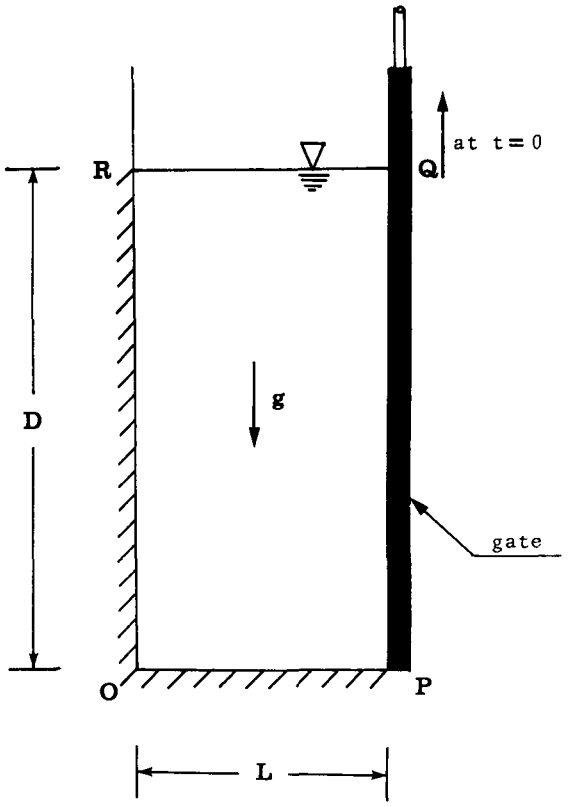

Figure 2. Problem definition for the broken dam problem

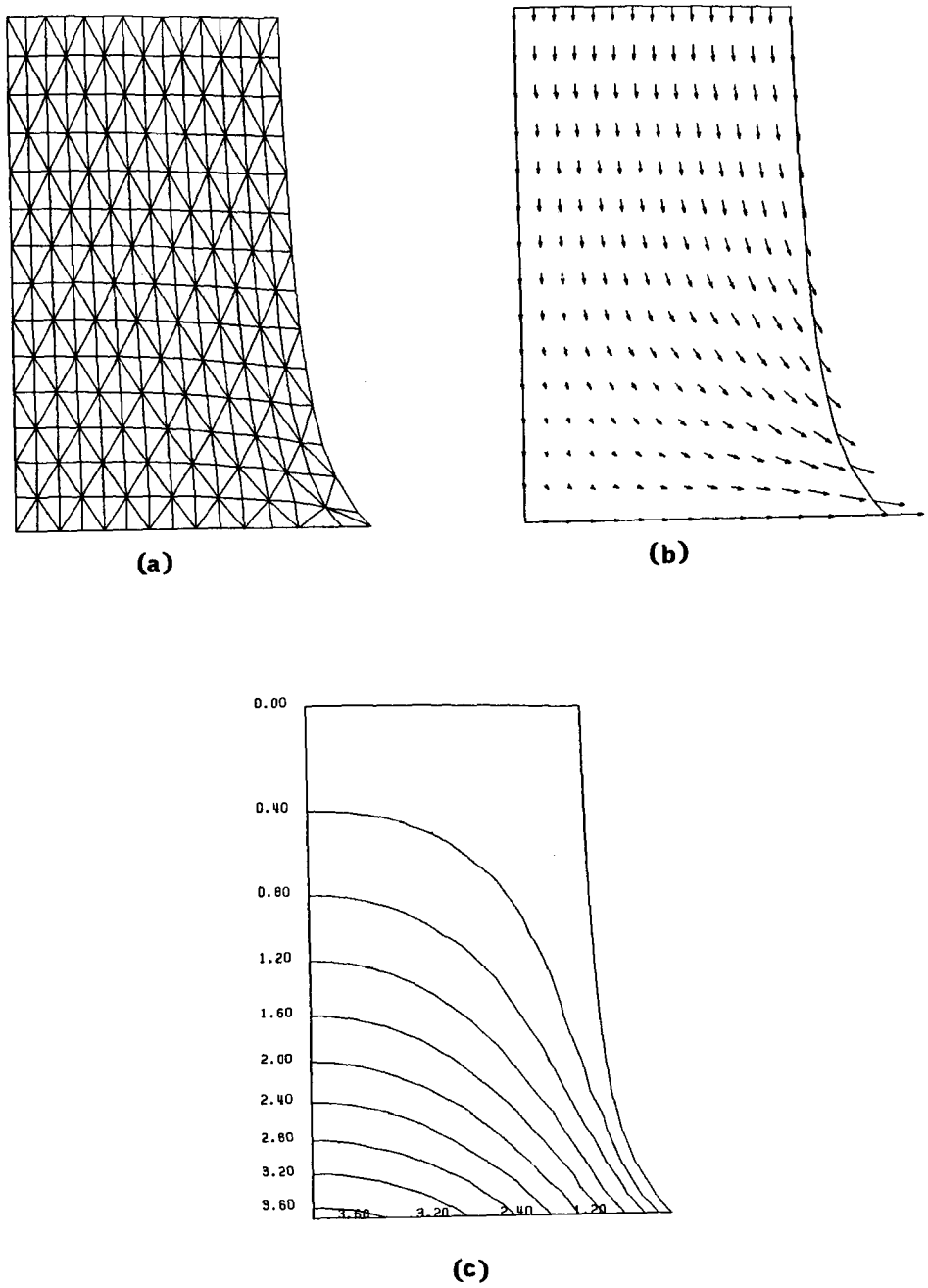

Figure 3. Computed results at time $t = 1{\cdot}0$: (*a*) mesh division; (*b*) velocity vectors; (c) pressure distribution

appearance of both a vertical and horizontal free surface, however, provides a check on the capability of the present Lagrangian approach to treat free surfaces that are not single-valued with respect to x_1 or x_2. The comparison of the computed results with those from experiments[23], plotted in Figure 8, shows close agreements in all respects.

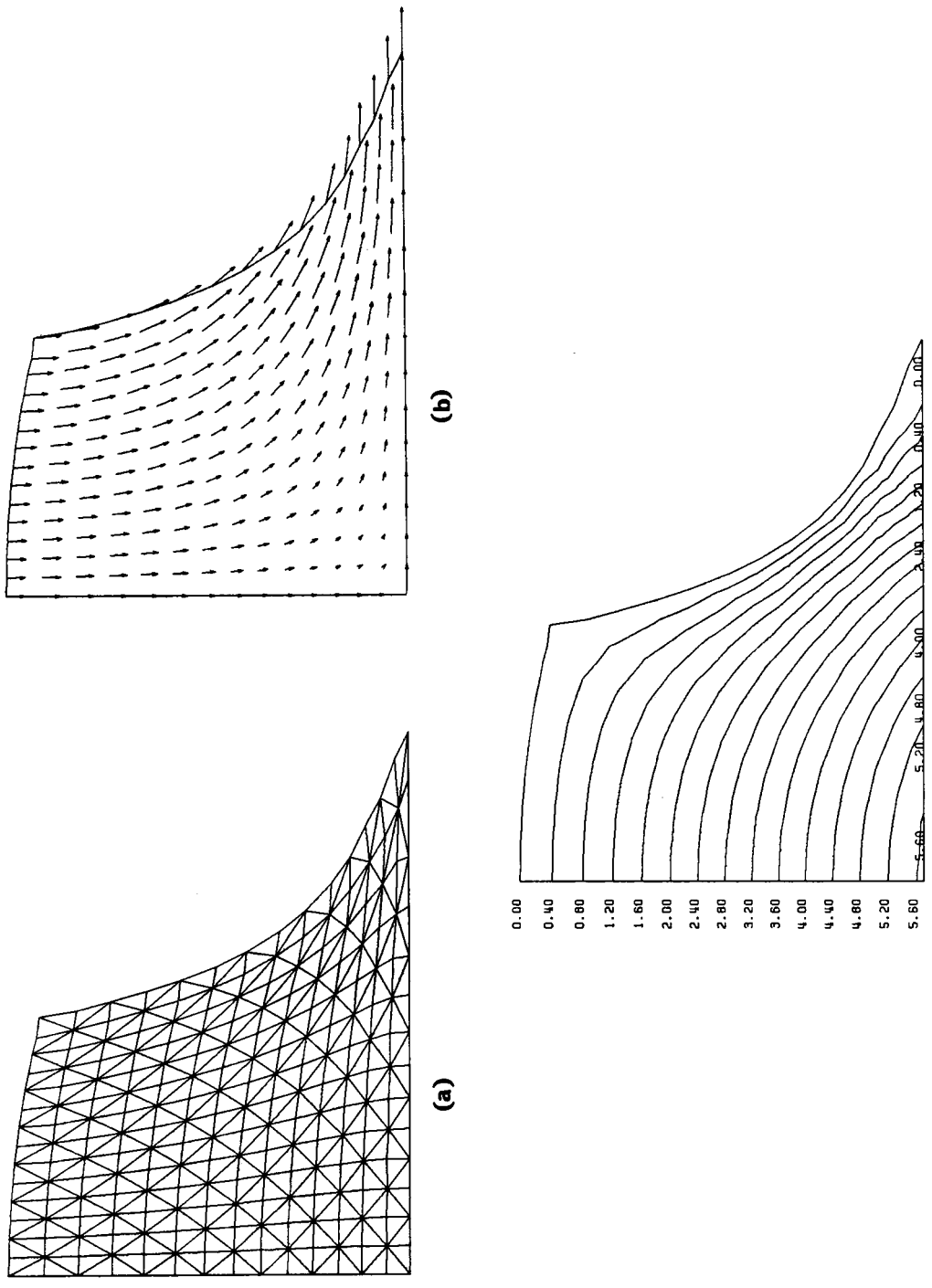

Figure 4. Computed results at time $t = 2.0$: (*a*) mesh division; (*b*) velocity vectors; (*c*) pressure distribution

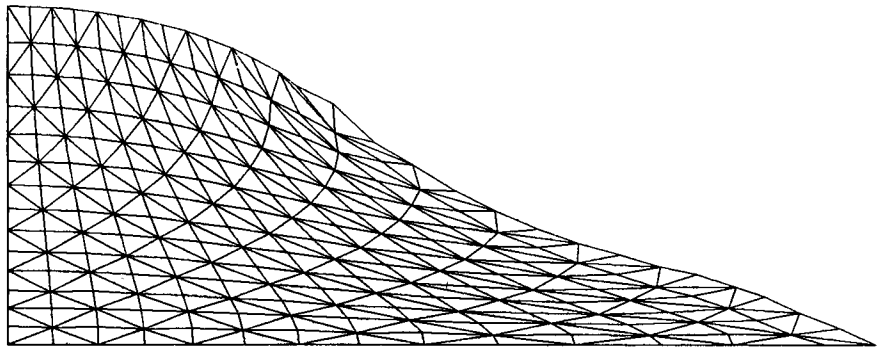

(a)

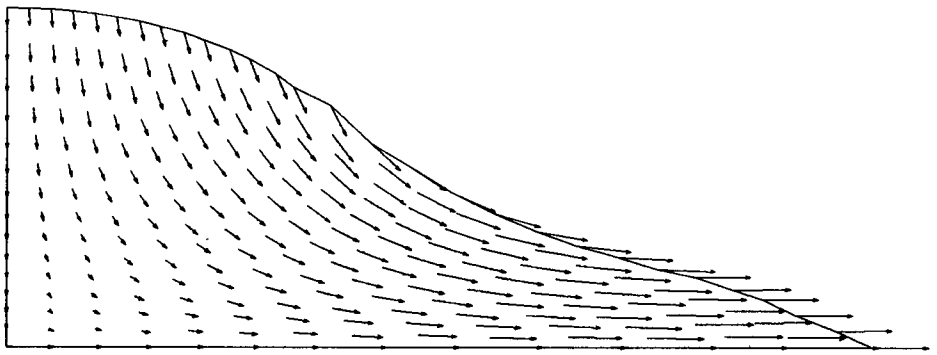

(b)

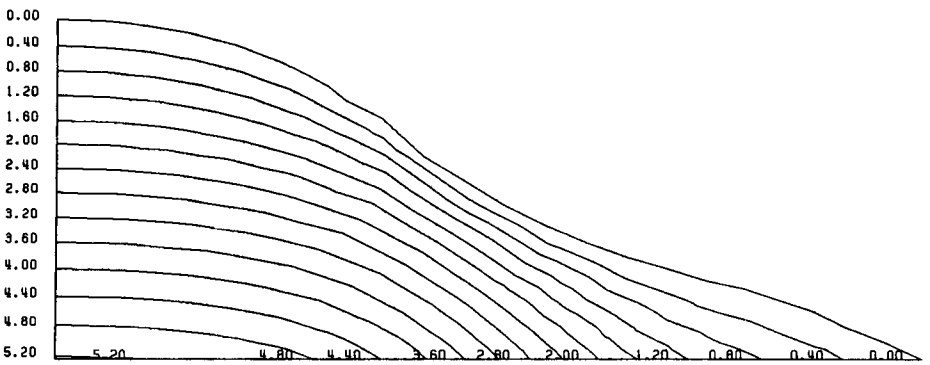

(c)

Figure 5. Computed results at time $t = 3{\cdot}0$: (*a*) mesh division; (*b*) velocity vectors; (*c*) pressure distribution

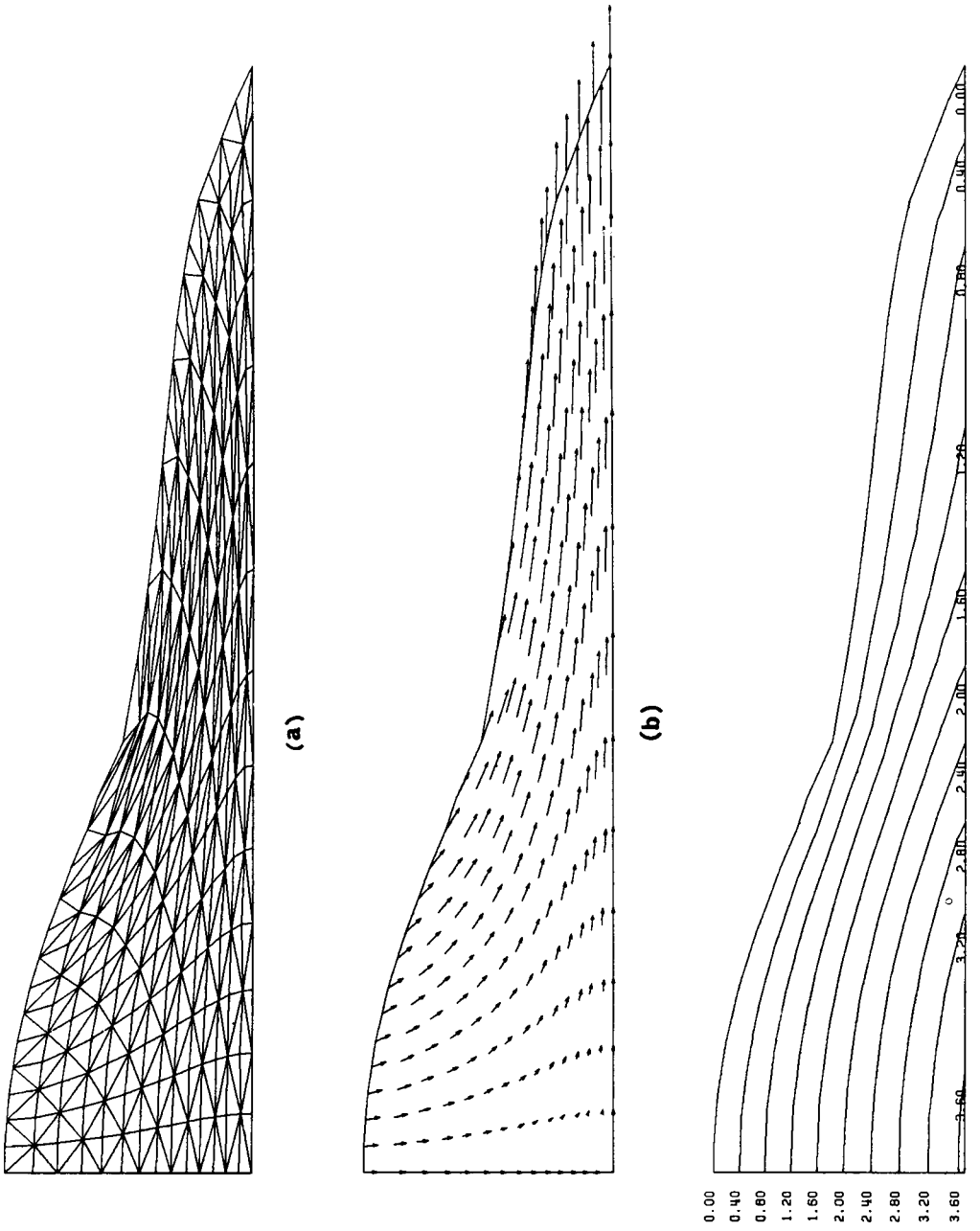

Figure 6. Computed results at time $t = 4{\cdot}0$: (*a*) mesh division; (*b*) velocity vectors; (*c*) pressure distribution

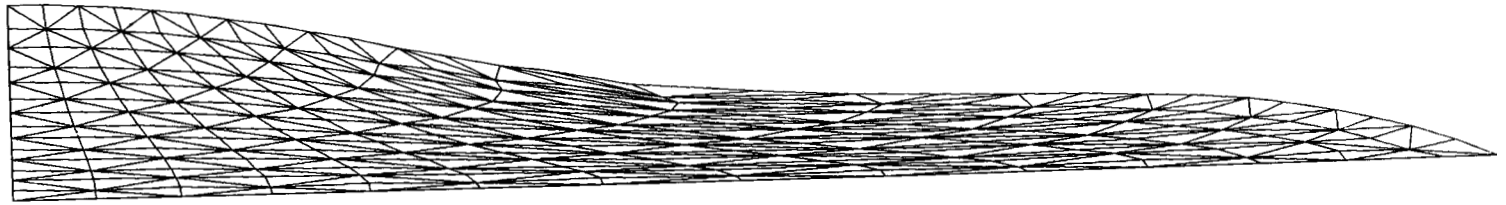

(a)

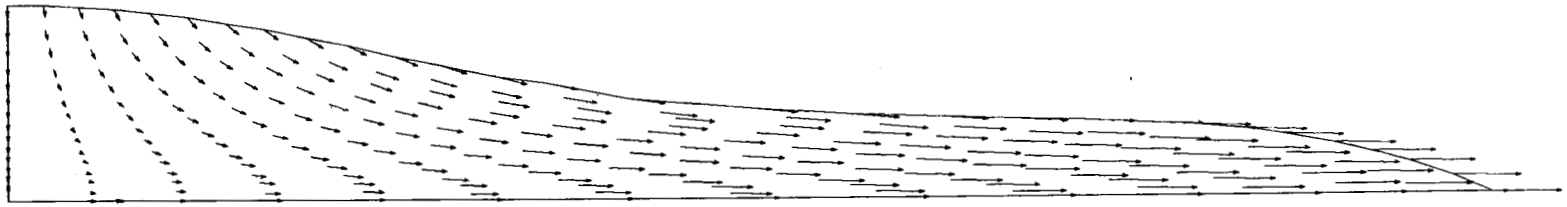

(b)

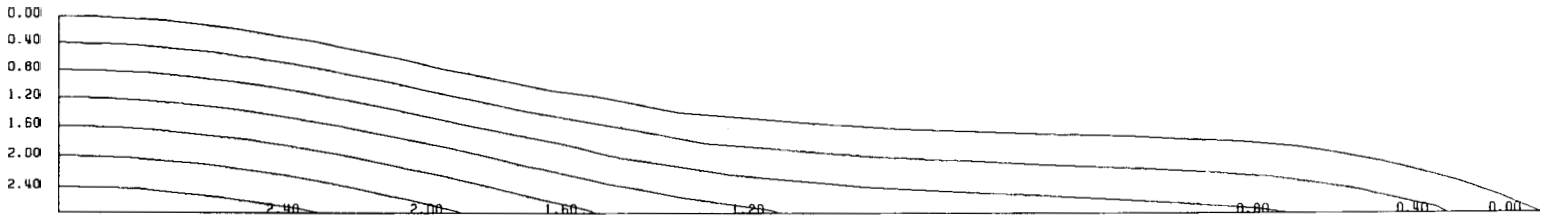

(c)

Figure 7. Computed results at time $t = 5{\cdot}0$: (*a*) mesh division; (*b*) velocity vectors; (*c*) pressure distribution

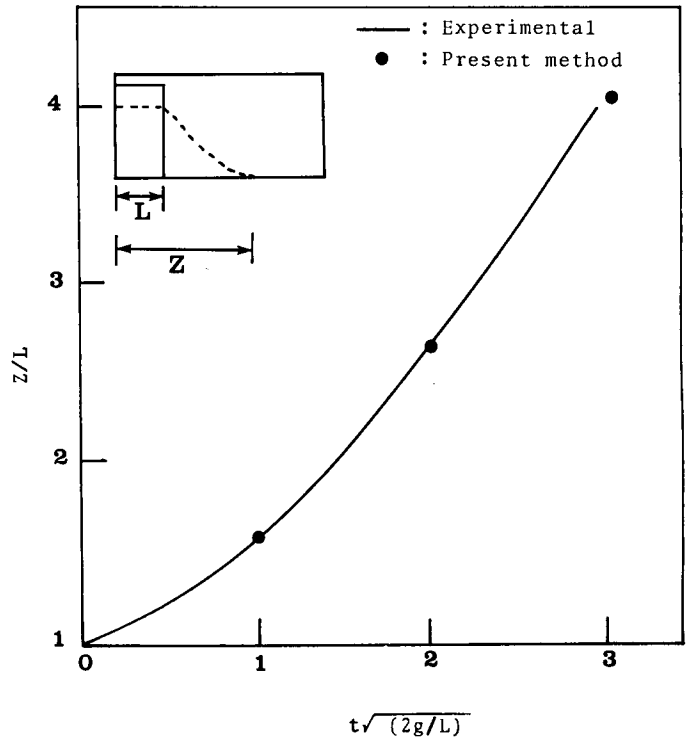

Figure 8. Comparison of calculated results with experimental data for the broken dam problem

Non-linear oscillation

This example has been chosen to demonstrate the validity of the present computing technique with highly non-linear effects. Fluid initially at rest in a rectangular tank is impulsively set into oscillation by a cosine pressure pulse applied at the free surface. The linear analysis for the change in surface elevation, η, above the initially undisturbed free surface height D gives

$$\eta = -A\sqrt{\left(\frac{\xi}{gD}\right)}\sin\left[t\sqrt{\left(\frac{g\xi}{D}\right)}\right]\cos(kx_1), \tag{53}$$

where

$$\xi = kD\tanh(kD). \tag{54}$$

Here $k = 2\pi/\lambda$, where λ is the disturbance wavelength and g is the acceleration of gravity. The initial pressure pulse on the free surface is described by

$$p(t) = A\delta(t)\cos(kx_1), \tag{55}$$

where $\delta(t)$ is the Dirac delta function.

A schematic view of the container used for the analysis is illustrated in Figure 9. In the present example, the fluid initially occupies a region 4.8 units wide and 4.0 units high. A gravity acceleration of one unit acts downwards and the amplitude of impulsive motion is assumed to be unity. The total numbers of nodal points and finite elements are 273 and 480 respectively. The calculation was performed with a viscosity of $v = 0{\cdot}01$ to compare the computed results with the MAC calculation.[24]

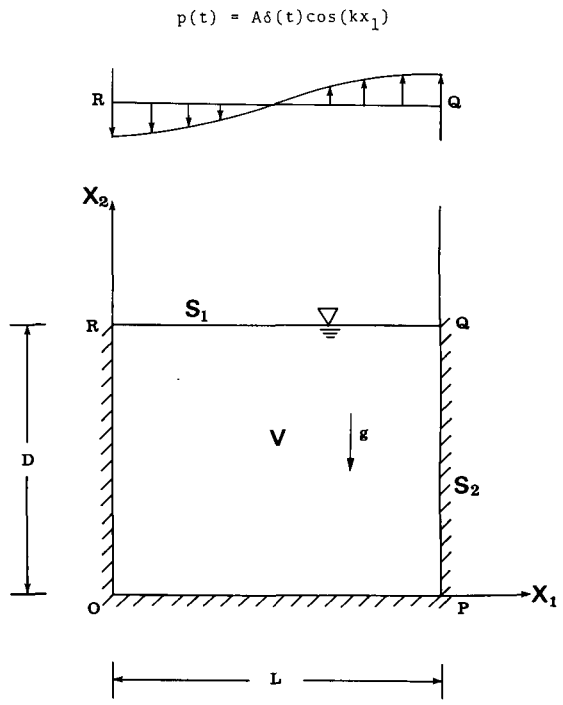

Figure 9. Problem definition for the oscillating flow problem

Calculated results for this problem are shown in Figures 10–13. Non-linear effects influence the amplitude of the surface, as indicated in Figure 13. The elevated portion of the surface, the spike, has a larger amplitude than the linear theory would suggest, while the depressed portion of the surface, the bubble, has a smaller amplitude. The comparison of the MAC and the present Lagrangian method is also shown in Figure 13. Close agreement have been obtained.

Rayleigh–Taylor instability problem

'Rayleigh–Taylor instability' refers to the principle that when two superposed fluids of different densities are accelerated in a direction perpendicular to their interface, this surface is stable or unstable according to whether the acceleration is directed from the heavier to the lighter fluid or *vice versa*. Since the present Lagrangian technique is applied to only one fluid with a free surface, the above definition is restated in the following manner. With gravity pointing downwards, out of the fluid, the free surface irregularities are unstable, which is known as 'Rayleigh–Taylor instability'. In every example, the pressure pulse was applied to the plane surface of a quiescent. The pressure pulse is given by equation (55).

In the first example, the fluid initially occupies a region 4·8 units wide and 2·0 units (shallow water) high, as shown in Figure 14. A gravity acceleration of one unit acts downwards and the amplitude of the impulsive motion is assumed to be $A = 5{\cdot}0$ (large impulse). The total numbers of nodal points and finite elements are 505 and 960 respectively. The calculation was performed with a viscosity of $\nu = 0{\cdot}01$. Figures 15–19 show a sequence of mesh configuration, velocity and pressure plots at a sequence of times, illustrating the growth of instability well into the spike and bubble phases. Figure 20 shows the surface displacement histories of the spike and bubble. From this

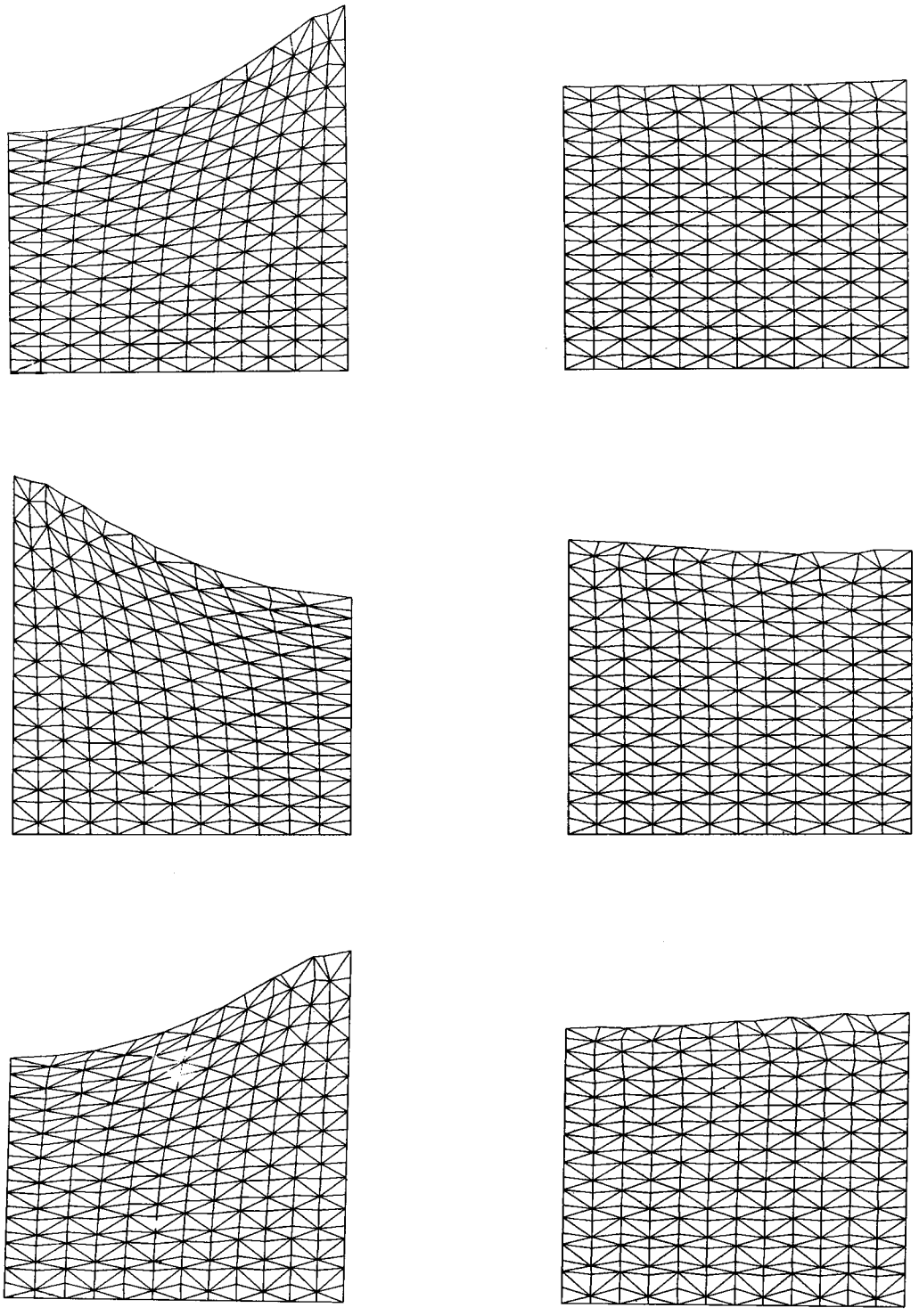

Figure 10. Mesh configuration in non-linear oscillation for the calculation with $A = 1{\cdot}0, D = 4{\cdot}0$. The times are 2·0, 4·0, 6·0, 8·0, 10·0, 12·0

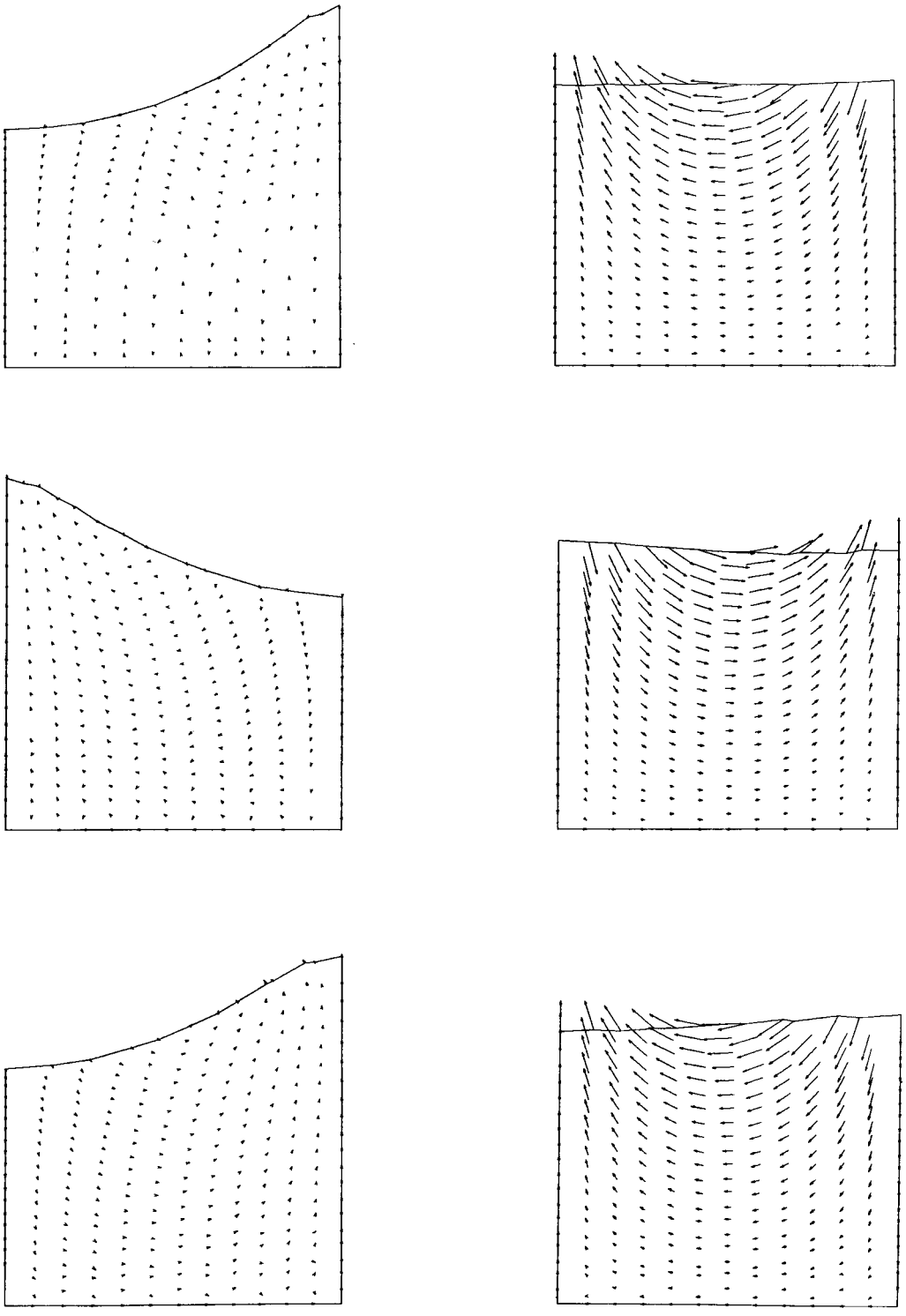

Figure 11. Velocity vectors corresponding to the frames shown in Figure 10

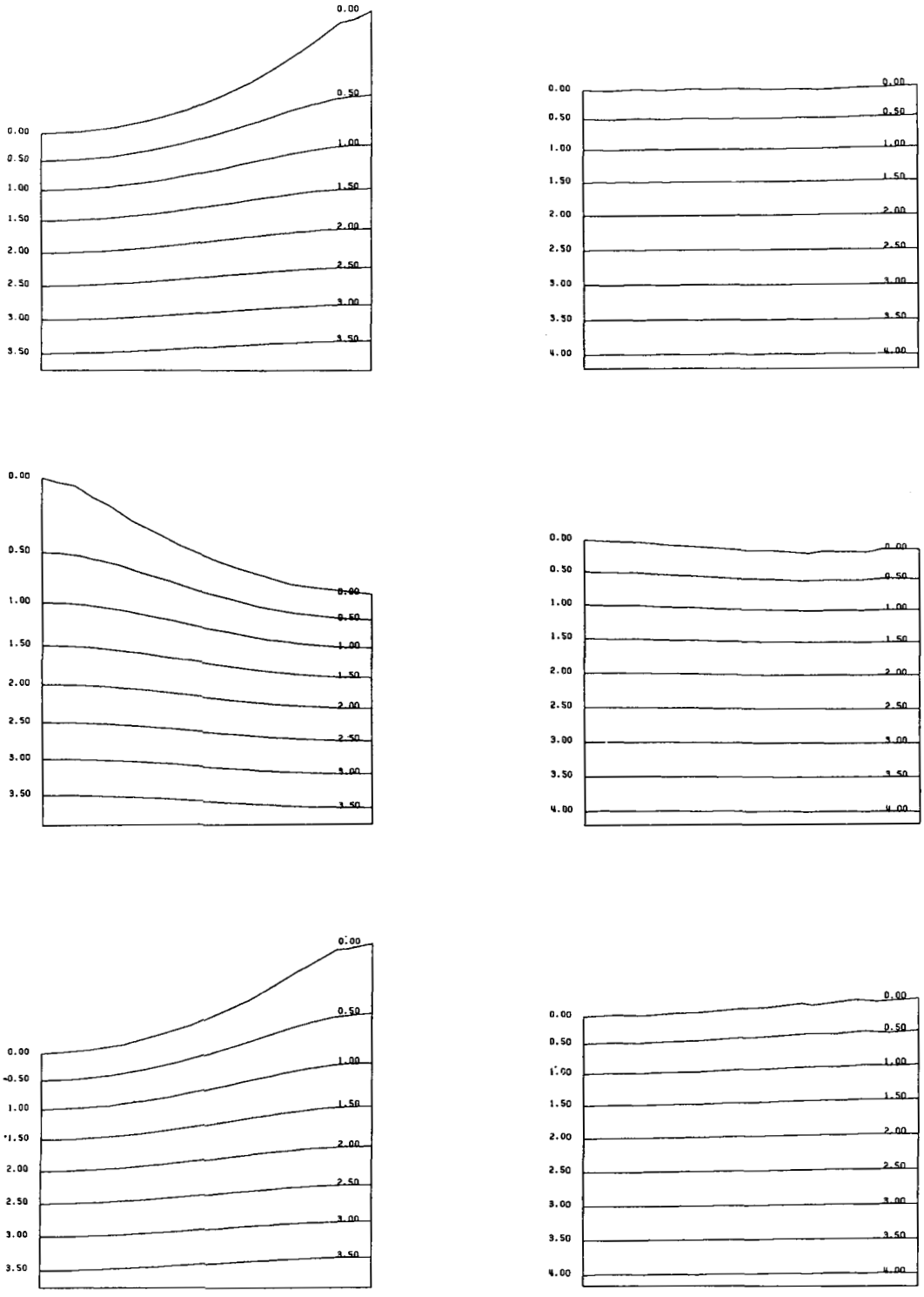

Figure 12. Pressure contours corresponding to the frames shown in Figure 10

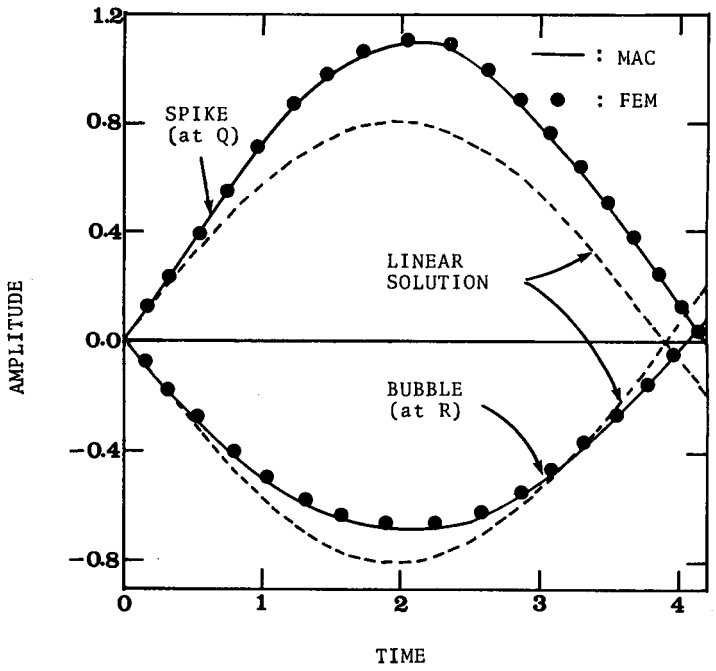

Figure 13. Amplitudes of spike and bubble as functions of time for the oscillating flow

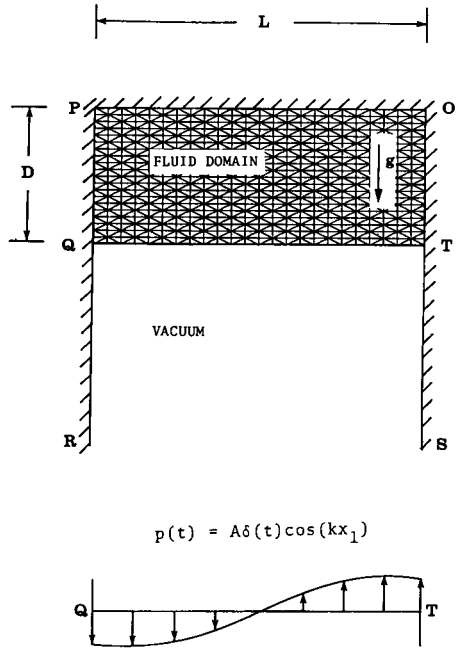

Figure 14. Problem definition for the Rayleigh–Taylor instability problem

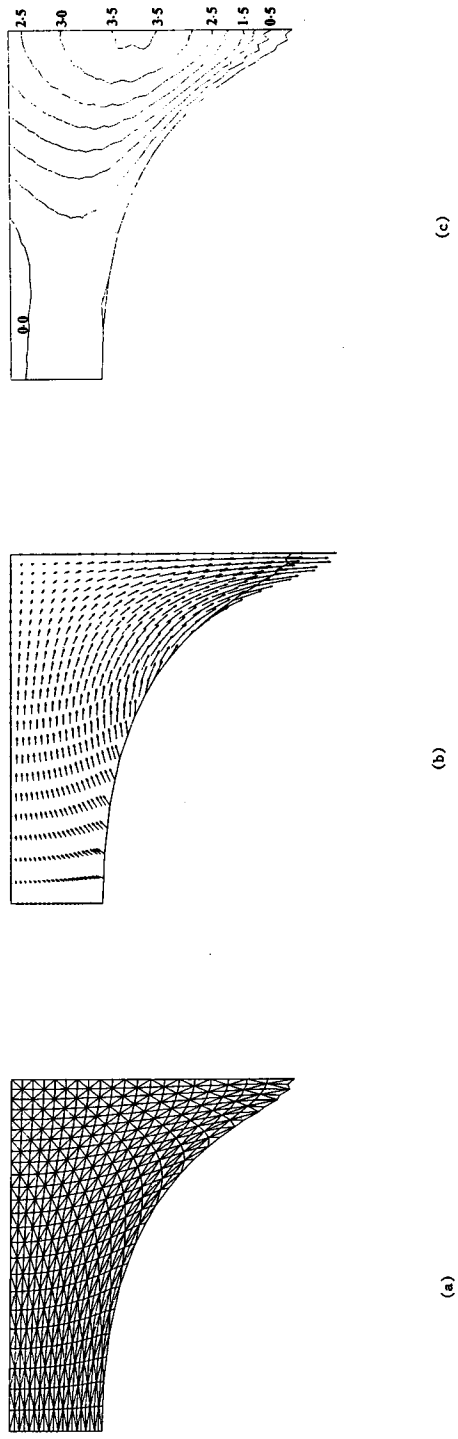

Figure 15. Computed results at time $t = 0{\cdot}4$: (*a*) mesh division; (*b*) velocity vectors; (*c*) pressure distribution

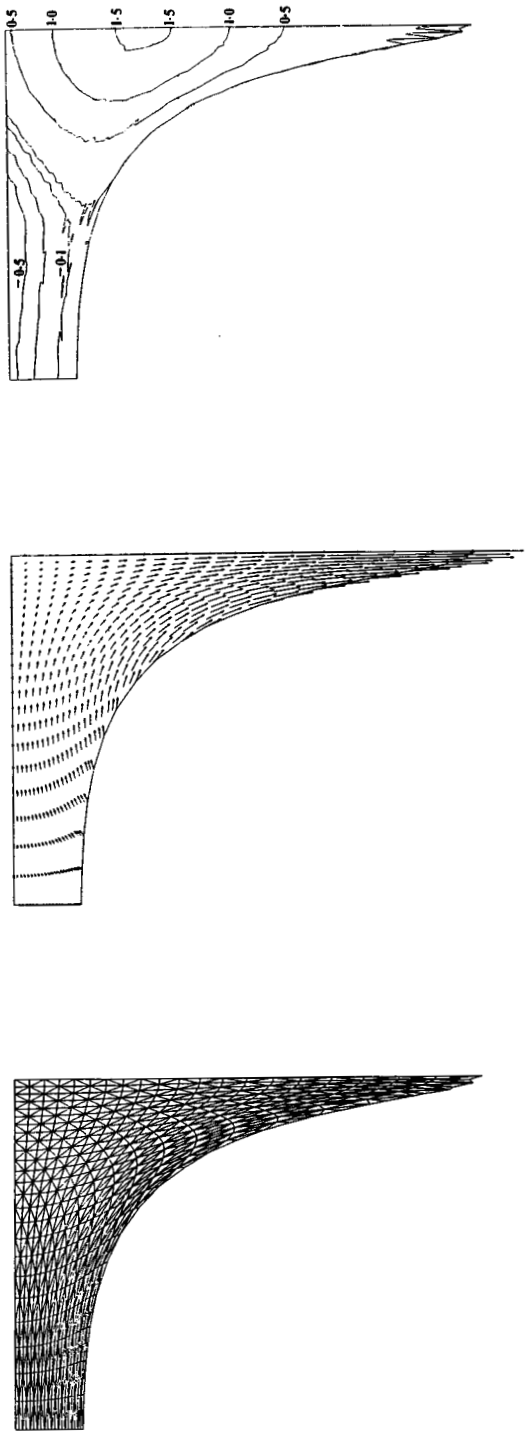

Figure 16. Computed results at time $t = 0{\cdot}8$: (*a*) mesh division; (*b*) velocity vectors; (*c*) pressure distribution

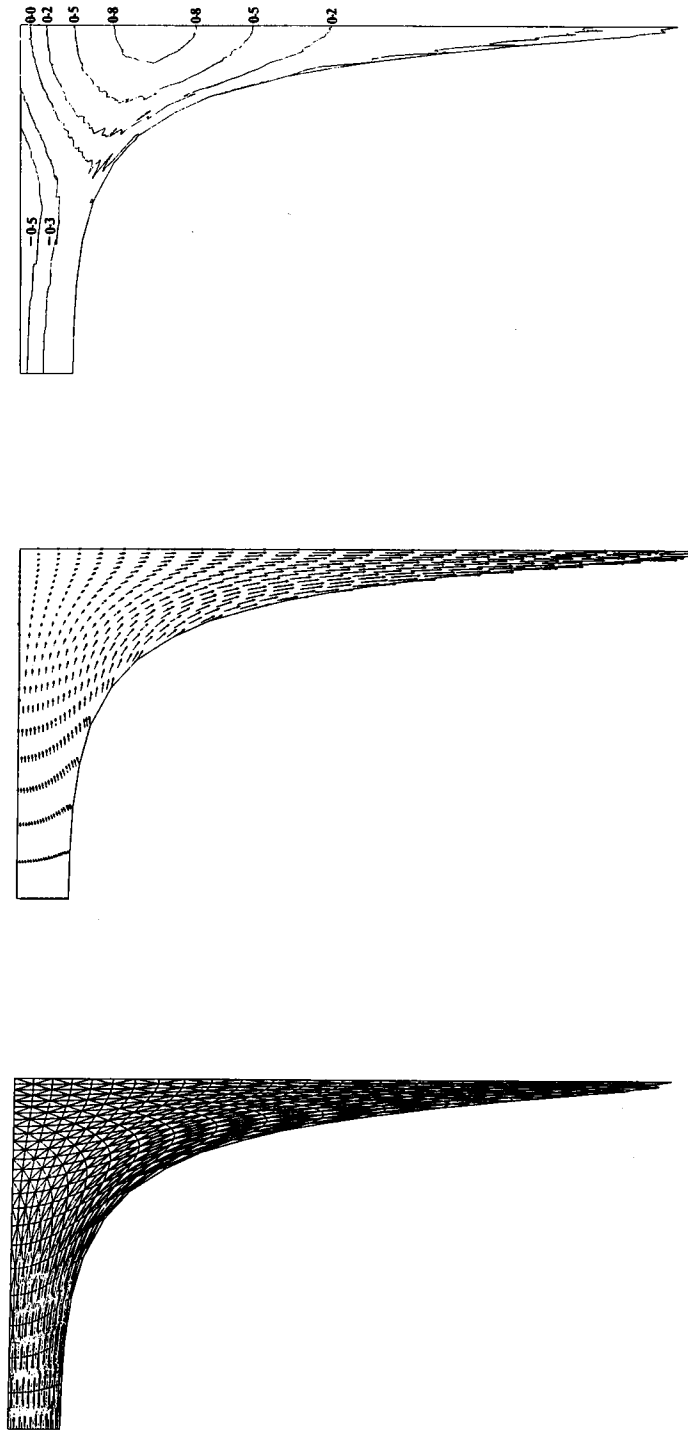

Figure 17. Computed results at time $t = 1{\cdot}2$: (*a*) mesh division; (*b*) velocity vectors; (*c*) pressure distribution

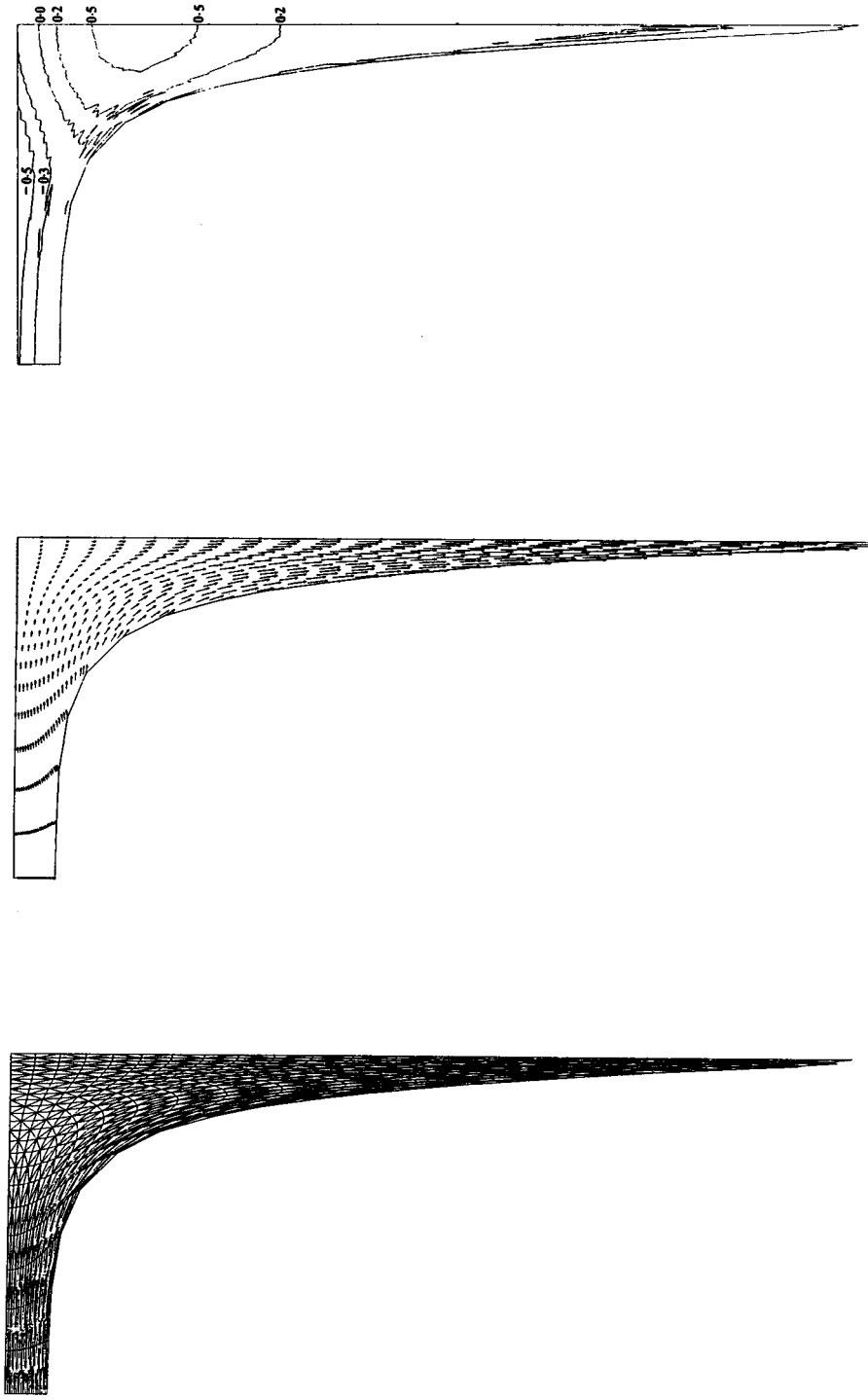

Figure 18. Computed results at time $t = 1{\cdot}6$: (*a*) mesh division; (*b*) velocity vectors; (*c*) pressure distribution

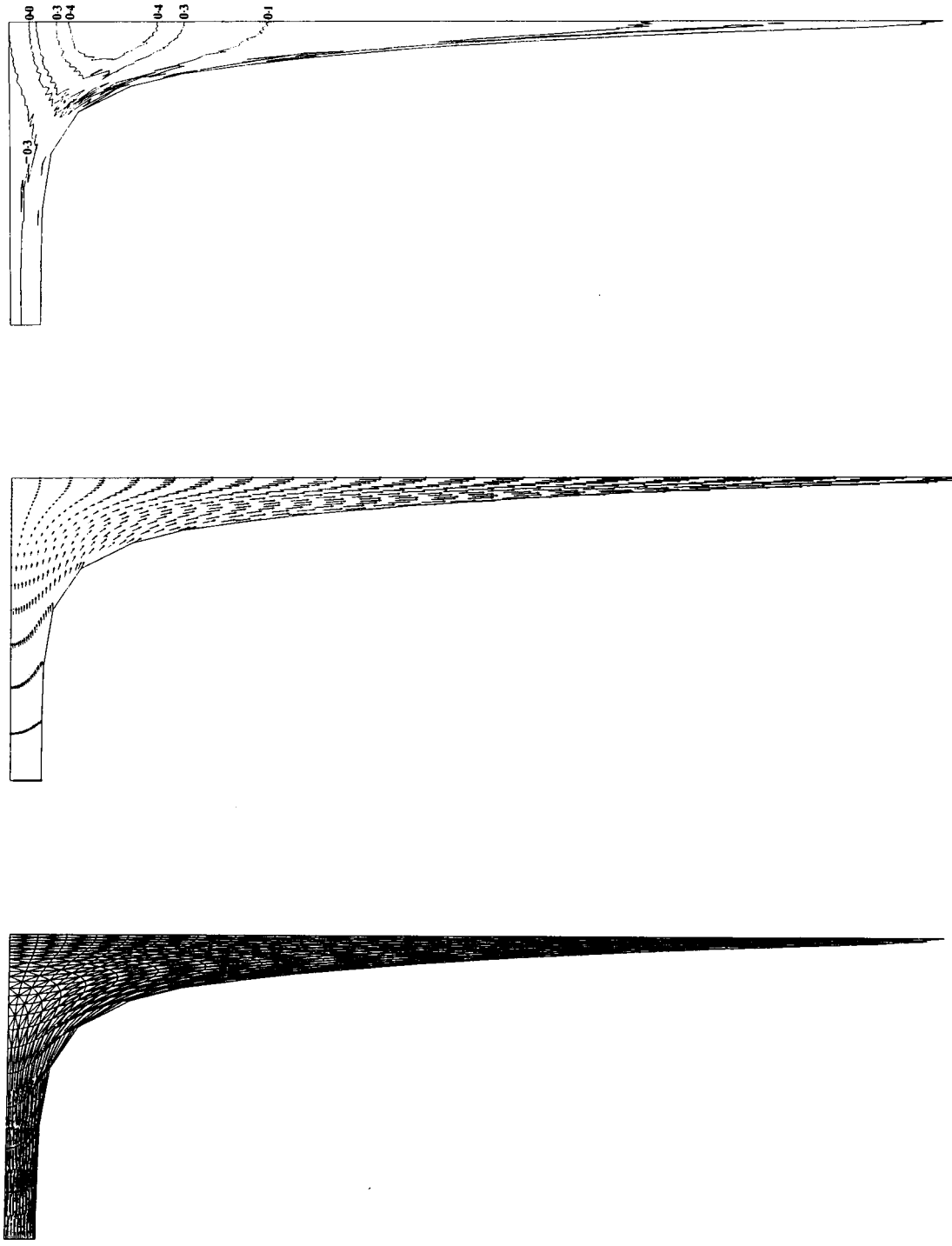

Figure 19. Computed results at time $t = 2{\cdot}0$: (*a*) mesh division; (*b*) velocity vectors; (*c*) pressure distribution

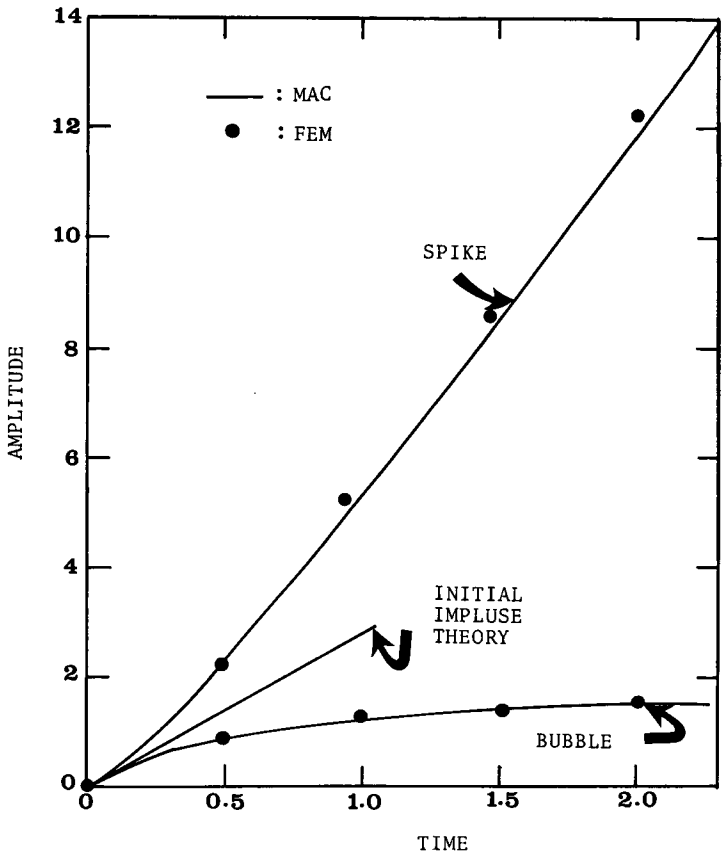

Figure 20. Amplitudes of spike and bubble as functions of time for calculation with $A = 5{\cdot}0, D = 2{\cdot}0$

figure, it can be seen that the spike, however, quickly reaches the free fall stage, as expected.

The results described in the last example are for a fluid whose depth is very shallow. In this example, the value of D is assumed to be 8·0 units (deep water), the conditions being otherwise identical to those for the calculation described in the last example. The total numbers of nodal points and finite elements are 273 and 480 respectively. The computed results are illustrated in Figure 21. Figure 22 shows the surface displacement histories of the spike and bubble, which clearly reflect the non-linear effects.

In the final example, the coefficient of viscosity is assumed to be $\nu = 2{\cdot}0$, the amplitude of the impulsive motion is $A = 0{\cdot}5$ and the other conditions are identical to the second example. The computed results are illustrated in Figure 23. A comparison between Figures 23 and 21 shows the viscous effect slowing the motion considerably, increasing the width of the spike and narrowing the bubble, so that the basic harmonic of the perturbation persists longer. Figure 24 shows the spike and bubble motions quantitatively.

CONCLUDING REMARKS

The conclusion from the work described in this paper are:

(1) A new computing technique and algorithm for using a Lagrangian two-dimensional mesh of triangles are described to represent and solve free surface problems in incompressible

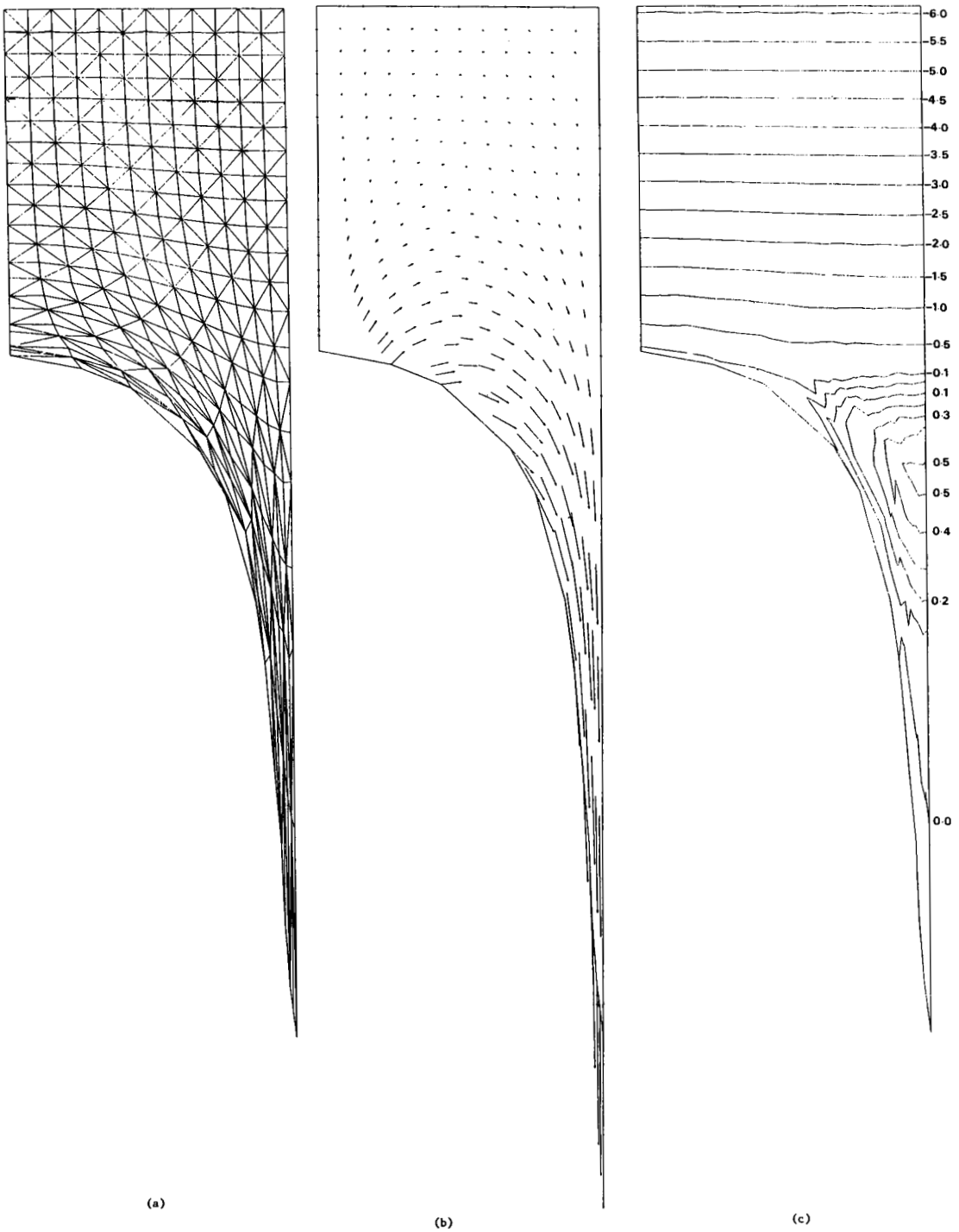

Figure 21. Computed results at time $t = 2{\cdot}5$: (*a*) mesh division; (*b*) velocity vectors; (*c*) pressure distribution

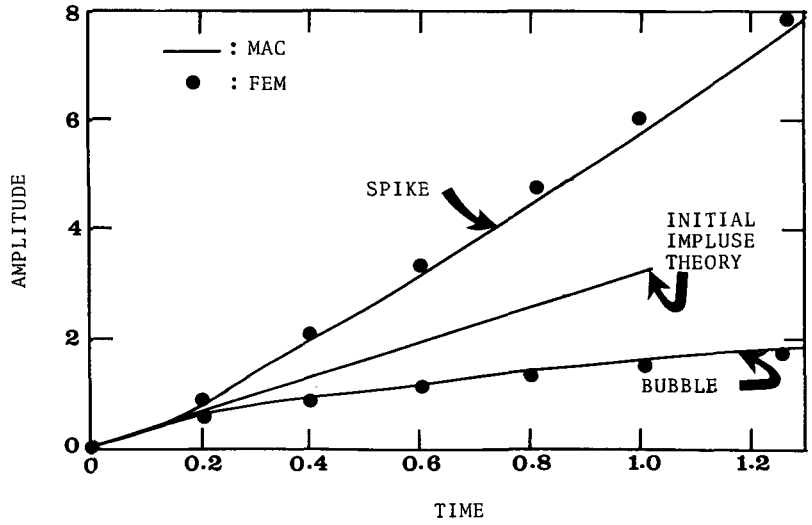

Figure 22. Amplitudes of spike and bubble as functions of time for calculation with $A = 5{\cdot}0, D = 8{\cdot}0, \nu = 0{\cdot}01$

hydrodynamics. The examples shown demonstrate the method's flexibility in terms of geometry and boundary conditions, as well as its robustness in obtaining solutions to difficult problems. In addition to the examples shown here, the authors have successfully applied this new finite element method based on Lagrangian specification to a number of other test cases.

(2) The proposed method uses Lagrangian specification for tracking the fluid motion, but solves the Eulerian equation of motion in a fashion similar to the MAC technique, which makes the treatment of free surfaces and material interfaces straightforward.

(3) The algorithm for the Lagrangian process consists of an outer time-stepping loop and inner co-ordinate iteration loop. By using proper time increments in the outer loop, the desired velocity in the inner loop can be made arbitrarily close to the known velocity in the previous time step.

(4) The present work shows that the use of the Lagrangian finite element method for free surface viscous flow problems is elegant and that results of acceptable accuracy can be produced with a reasonable expenditure of computing effort. It also has the ability to calculate long-time solutions accurately without the benefit of artificial or numerical averaging. In addition, it is very easy to modify for multi-material studied and the incorporation of surface tension effects.

(5) The iterative solution methods used in the current formulation provide considerable savings in computer execution times and storage requirements compared with other finite element methods. This saving allows the new Lagrangian formulation to be competitive with existing finite difference methods, while maintaining the traditional geometric flexibility of finite elements.

(6) The present computing technique provides a viable computational method for solving problems with equality of representation of the pressure and velocity fields. Its success has been attributed to the strict enforcement of the continuity constraint at every stage of the iterative process. This approach is not affected by the spurious phenomenon of spatial oscillations of the pressure, the so-called chequer-board splitting encountered in some other studies.

(7) In general, the Lagrangian formulation is very useful for problems not involving large distortions, but requiring an accurate knowledge of free fluid boundaries.

(8) Work is currently underway to develop this method further in a number of areas. These areas include: the extension to three-dimensional geometries, coupled fluid/thermal problems and mixed Lagrangian–Eulerian descriptions to deal with problems involving free boundaries.

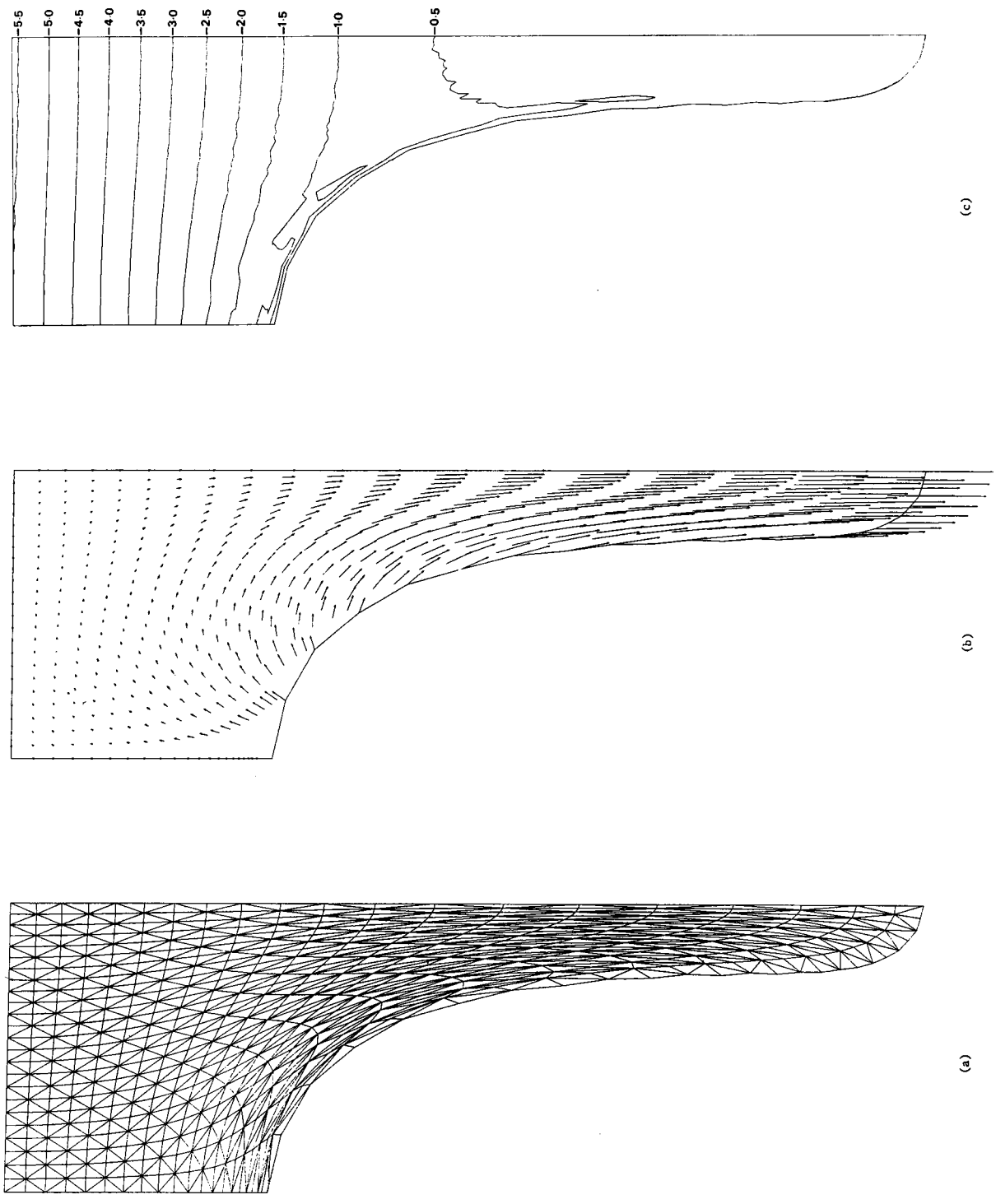

Figure 23. Computed results at time $t = 8{\cdot}5$: (*a*) mesh division; (*b*) velocity vectors; (*c*) pressure distribution

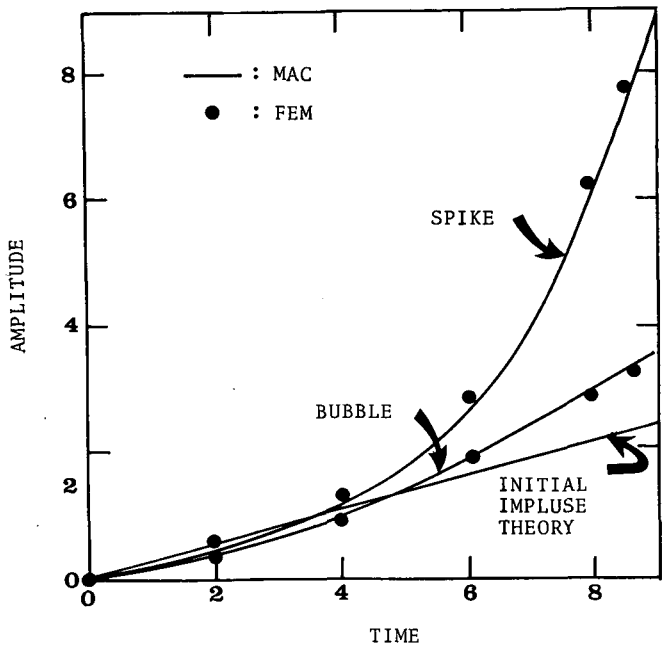

Figure 24. Amplitude of spike and bubble as functions of time for calculation with $A = 0{\cdot}5$, $D = 8{\cdot}0$, $v = 2{\cdot}0$

ACKNOWLEDGEMENTS

The authors wish to thank Dr. T. Nakayama of Chuo University for his interest, encouragement and many helpful discussions. The computation has been carried out using the FACOM M170F of Chuo University and the HITAC M680H of the University of Tokyo.

REFERENCES

1. F. H. Harlow and J. E. Welch, 'Numerical calculation of time-dependent viscous incompressible flow of fluid with free surface', *Phys. Fluids*, **8**, 2182–2189 (1965).
2. F. H. Harlow, J. P. Shannon and J. E. Welch, 'Liquid waves of computer', *Science*, **149**, 1092 (1965).
3. J. E. Welch, F. H. Harlow, J. P. Shannon and B. J. Daly, 'The MAC method: a computing technique for solving viscous, incompressible, transient fluid-flow problems involving free surfaces', *Report LA-3425*, Los Alamos Scientific Laboratory, 1966.
4. C. W. Hirt, J. L. Cook and T. D. Butler, A Lagrangian method for calculating the dynamics of an incompressible fluid with free surface', *J. Comput. Phys.*, **5**, 103–124 (1970).
5. A. A. Amsden and F. H. Harlow, 'A simplified MAC technique for incompressible fluid flow calculations', *J. Comput. Phys.*, **6**, 322–325 (1970).
6. R. K.-C. Chan and R. L. Street, 'A computer study of finite-amplitude water waves', *J. Comput. Phys.*, **6**, 68–94 (1970).
7. R. E. Nickell, R. I. Tanner and B. Caswell, 'The solution of viscous incompressible jet and free-surface flows using finite element method', *J. Fluid. Mech.*, **65**, 189–206 (1974).
8. K. R. Reddy and R. I. Tanner, 'Finite element solution of viscous jet flows with surface tension', *Comput. Fluids*, **6**, 83–91 (1978).
9. F. M. Orr and L. E. Scriven, 'Rimming flow: numerical simulation of steady, viscous, free-surface flow with surface tension', *J. Fluid. Mech.*, **84**, 145–165 (1978).
10. B. J. Omodei, 'Computer solutions of a plane Newtonian jet with free surface tension', *Comput. Fluids*, **7**, 79–96 (1986).
11. W. J. Silliman and L. E. Scriven, 'Separating flow near a static contact line: slip at a wall and shape of a free surface', *J. Comput. Phys.*, **34**, 287–313 (1980).
12. K. J. Ruschak, 'A method of incorporating free boundaries with surface tension in finite element fluid flow simulations', *Int. j. numer. methods eng.*, **15**, 639–648 (1980).
13. H. Saito and L. E. Scriven, 'Study of coating flow by the finite element method', *J. Comput. Phys.*, **42**, (1981).
14. H. S. Kheshgi and L. E. Scriven, 'Penalty finite element analysis of time-dependent two-dimensional free surface film

flows', in T. Kawai (ed.), *Finite Element Flow Analysis*, University of Tokyo Press, 1982, pp. 113–120.
15. L. E. Scriven and S. F. Kistler, 'Coating flow theory by finite element and asymptotic analysis of Navier–Stokes system', in T. Kawai (ed.), *Finite Element Flow Analysis*, University of Tokyo Press, 1982, pp. 503–510.
16. F. Dupret, 'A method for the computation of viscous flow by finite elements with free boundaries and surface tension', in T. Kawai (ed.), *Finite Element Flow Analysis*, University of Tokyo Press, 1982, pp. 495–502.
17. P. Bach and O. Hassager, 'An algorithm for the use of the Lagrangian specification in Newtonian fluid mechanics and applications to free-surface flow', *J. Fluid Mech.*, **152,** 173–190 (1985).
18. L. C. Wellford and T. H. Ganaba, 'A finite element method with hybrid Lagrange line for fluid mechanics problems involving large free surface motion', *Int. j. numer. methods eng.*, **17,** 1201–1231 (1981).
19. C. S. Frederiksen and A. M. Watts, 'Finite element method for time-dependent incompressible free surface flow', *J. Comput. Phys.*, **39,** 282–304 (1981).
20. M. Kawahara and T. Miwa, 'Finite element analysis of wave motion', *Int. j. numer. methods eng.*, **20,** 1193–1210 (1984).
21. R. K.-C. Chan, 'A discretized solution for the solitary waves', *J. Comput. Phys.*, **16,** 32–48 (1974).
22. K. Washizu, T. Nakayama and M. Ikegawa, 'Application of the finite element method to some free surface fluid problems', in W. G. Gray *et al.* (eds), *Finite Elements in Water Resources*, Pentech Press, London, 1978, pp. 247–266.
23. C. W. Hirt and B. D. Nichols, 'Volume of fluid (VOF) method for the dynamics of free boundaries', *J. Comput. Phys.*, **39,** 1981, pp. 201–225.
24. F. H. Harlow and J. E. Welch, 'Numerical study of large-amplitude free-surface motions', *Phys. Fluids*, **9,** 842–851 (1966).